# Structural, morphological, and optical properties of praseodymium and aluminium codoped ZnO nanoparticles

M. S. Viswaksenan[a,b], A. Simi[c*], A. Panneerselvam[d]
[a] *Research Scholar, PG & Research Department of Chemistry, St.Josephs college (Autonomous), Affiliated to Bharathidasan university, Tiruchirappalli-620 002, Tamilnadu, India*
[b] *Department of Chemistry, Vivekanandha college of Engineering for women (Autonomous), Tiruchengode-637205, Tamilnadu, India*
[c] *PG & Research Department of Chemistry, St.Josephs college (Autonomous), Tiruchirapalli-620002, Tamilnadu, India*
[d] *Department of Physics, Vivekanandha college of Engineering for women (Autonomous), Tiruchengode-637205, Tamilnadu, India*

Using a soft chemical process that involves nitrates and heat annealing, nanoparticles of undoped ZnO and praseodymium, aluminum-codoped ZnO may be produced. XRD, SEM with EDS, and FTIR analysis determine nanocatalyst structures, morphologies, and chemical bonding. PL and UV spectroscopy examines optical characteristics. The peak in the FTIR spectral line at 714 $cm^{-1}$ in the study indicates M-O stretching in the samples and ZnO's interaction with the Pr and Al matrix. XRD patterns indicated prepared nanoparticles with nanosizes ranging from 40.07 to 38.65 to 36.84 to 38.87 to 39.91 nm. SEM analyzed nanoparticle size, shape, and interaction with the Pr and Al matrix. EDS determined NPs purity. UV-vis spectra of ZnO-Pr/Al nanocomposites showed UV absorption similar to ZnO nanoparticles. Doping ZnO with Pr and Al shrinks the bandgap and slows photogenerated electron-hole pair recombination without changing its crystalline structure.

(Received March 15, 2023; Accepted July 4, 2023)

*Keywords:* Zinc, Praseodymium, Aluminium, Photoluminescence

## 1. Introduction

Zinc oxide is widely considered to be one of the most important semiconductor materials. The most significant contributors to this phenomenon were the enormous excitonic binding energy of 60 meV and the significant direct band gap of 3.37 eV. The most frequent form of Wurtzite may be found in crystal structures containing zinc oxide [1,2]. ZnO has become a compelling material as a result of its many useful properties and impressive applications in fields as diverse as optoelectronics, reflection coatings, solar cells, anode-materials, gas-sensors, light-emitting diodes (LED), impact on biological activities, antibacterial actions, and drug delivery, and so on [3,4]. In terms of UV transmission and thermal stability at room temperature, zinc oxide surpassed both GaN and phosphorus[5]. Zinc oxide also fared better than GaN. In order to enhance surface acoustic wave filters, also known as SAW filters, which are often employed in audio and video frequency circuits, zinc oxide nanoparticles have been put to use[6]. Nanostructures made of zinc oxide have been fabricated by researchers, and they have shown exceptional light emission capabilities. In addition, zinc oxide was a chemical that had been well characterised and has obvious attraction to biological systems [7,8]. The majority of the time, the inclusion of rare earth metal ions results in an improvement of the properties like electrical and optical characteristics. Rare earth metals such as europium (Eu), gadolinium (Gd), yttrium (Yi), neodymium (Nd), samarium (Sm), and praseodymium (Pr) are co-doped with the ZnO to achieve even greater enhancements in the film's opto-electrical properties. In addition, the absorption of light at shorter wavelengths and the emission of light at longer wavelengths may be used by rare-earth metals to increase the

* Corresponding author: viswaksenan2u@gmail.com
https://doi.org/10.15251/JOR.2023.194.351

transparency of a material[9]. Pr is an important rare earth element because it can be readily incorporated into the ZnO structure to increase electrical conductivity. This is due to the fact that doped rare earth ions can be employed as down shifting layers within the electronic band structure to enhance their electrical behaviour[10]. As a result, Pr can be readily incorporated into the ZnO structure to increase electrical conductivity. Due to the fact that the ionic radius of $Pr^{3+}$(1.01) is greater than the ionic radii of $Al^{3+}$(0.54) and $Zn^{2+}$(0.54), it is possible for Pr ions to quickly replace the Al and Zn ions with just a little amount of alteration to the structure of the host ZnO(0.74). The creation of nanomaterials may be accomplished using a variety of processes, including thermal decomposition, hydrothermal synthesis, co-precipitation, chemical vapour deposition, spin coating technique, and others. The soft chemical technique was chosen for the synthesis of NPs because of its cheap cost and stability throughout a broad variety of environmental conditions (including swings in temperature and pressure)[11]. The synthesised NPs demonstrated a remarkable alteration in size, shape, and even optical features as a result of these characteristics[12]. The aforementioned characteristics may also be improved upon in nano-Zinc structures, nanoparticles, and nanowires, hence opening the way for an enhancement in the quality of exciton oscillators and an increase in quantum efficiency[13,14]. In this paper, Al and Pr codoped ZnO samples are synthesised via a soft chemical method and in order to examine the materials and establish their characteristics, X-ray diffraction (XRD), scanning electron microscopy (SEM) with energy dispersive x-ray emission spectroscopy (EDS), and Fourier transform infrared spectroscopy (FTIR) were all used. In order to evaluate the optical features, spectroscopic techniques such as photoluminescence (PL) and ultraviolet-visible (UV-vis) are used. The output from the synthesised NPs might be used in a wide variety of fields, including luminescence, optoelectronics, and displays.

## 2. Preparation of praseodymium and Aluminium codoped ZnO NPs

Zinc nitrate (0.98M), praseodymium nitrate hexahydrate (0.01), and aluminium nonahydrate (0.01M) were individually diluted in 100 cc of distilled water while vigorously swirling the solution. After that, the primary mixture was added to 25 mL of 2M NaOH in a drop-by-drop manner while the container was continually stirred. When the mixture is stirred continuously, a white precipitate forms. When the precipitate had been separated from the rest of the mixture, it was washed repeatedly in double-distilled water and ethanol. After that, the completed item was annealed for three hours at 450 degrees and dried in the oven for one hour at 100 degrees. Powder was made out of the obtained nanoparticles, and then the jar containing the powder was put away for safekeeping. The procedure was the same regardless of whether we were working with $Pr_{0.02}Al_{0.02}Zn_{0.96}O$, $Pr_{0.03}Al_{0.03}Zn_{0.94}O$ and $Pr_{0.04}Al_{0.04}Zn_{0.92}O$. The undoped ZnO NPs were produced using zinc nitrate at a concentration of 0.1M and sodium hydroxide at a concentration of 2.0M [15,16].

## 3. Result and discussion

### 3.1. X-ray diffraction analysis (XRD)

The XRD patterns of pure ZnO and Pr, Al-doped ZnO semi-conductor nanoparticles are shown in Figure 1. As shown by the existence of diffraction peaks corresponding to the (100), (002), and (101) planes, the nanocomposite material that was produced had a polycrystalline structure (Zincite, JCPDS: 36-1451). Indicating that wurtzite, which has its c-axis favoured to be perpendicular to the surface, was the primary component in the nanocomposite that developed, the strongest peak was detected at 34.5 degrees. In addition, there were no peaks created for PrO and AlO, which suggests that the only metal oxides that were present were Pr, Al codoped ZnO NPs and not any other types of metal oxides. For the purpose of determining the typical crystallite size of pure ZnO, $Pr_{0.02}Al_{0.02}Zn_{0.96}O$, $Pr_{0.03}Al_{0.03}Zn_{0.94}O$ and $Pr_{0.04}Al_{0.04}Zn_{0.92}O$ NPs, the Scherrer equation (1) was used,

$$D=K\lambda / (\beta \cos \theta) \quad (1)$$

The crystals that were grown had average nanosizes of 40.07, 38.65, 36.84, 38.87 and 39.91 nm when they were prepared. The reduction in size of Pr, Al codoped ZnO crystallites was attributed to the incorporation of $Pr^{2+}$ and $Al^{3+}$ into the ZnO matrix. On the other hand, the increased size of Pr, Al codoped ZnO NPs was attributed to a high number of defects brought about by the increased concentration of $Pr^{2+}$ ions in the Al-ZnO structure.

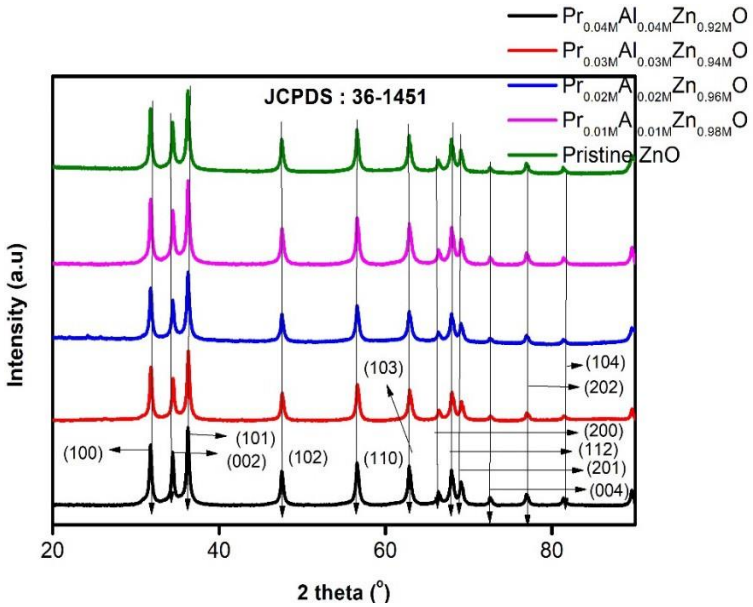
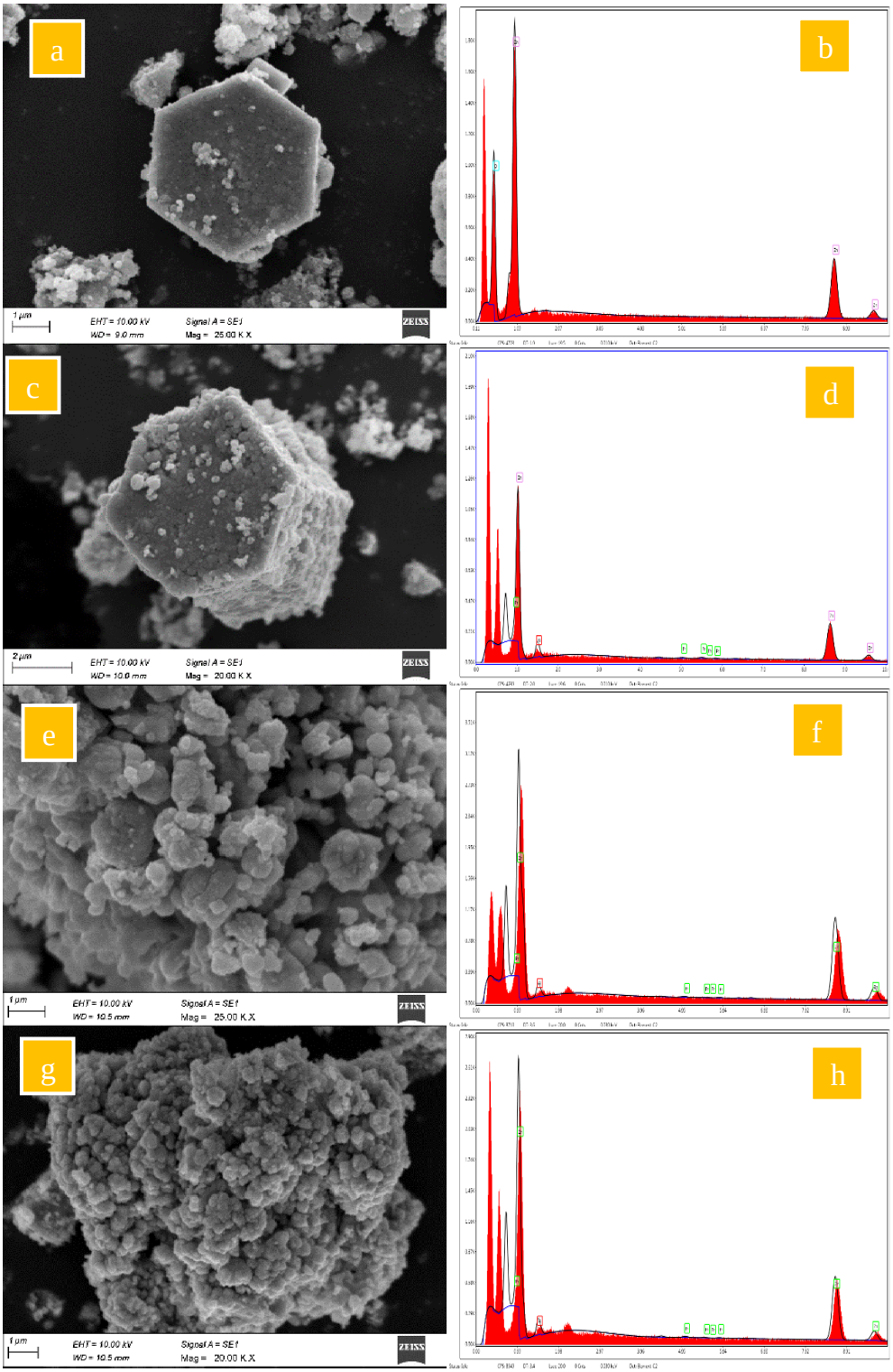



*Fig. 1. XRD image of prepared nanoparticles.*

### 3.2. Scanning Electron Microscope (SEM) and Energy Dispersive Studies (EDS)

In contrast to the undoped system, the nanoparticles formed by the Pr, Al codoping of ZnO are found to have a different shape in the SEM and EDAX photographs that are shown in Figure 2. The nanoparticles had an average size of fifty nanometers (nm). The nanoparticles that were produced were erratic in terms of both their size and their form[17]. EDAX analysis revealed that the atoms of aluminium, zinc, and oxygen were really present in the Pr, Al-ZnO nanoparticles. The EDAX scan did not reveal any oxygen-atom peaks that were distinct from those of the ZnO system, which is evidence that no additional metal oxides had formed. The results of the XRD examination supported the validity of this information as well.


a
b
c
d
e
f
g
h
1 µm
EHT = 10.00 kV
WD = 9.0 mm
Signal A = SEI
Mag = 25.00 K X
2 µm
EHT = 10.00 kV
WD = 10.0 mm
Signal A = SEI
Mag = 20.00 K X
1 µm
EHT = 10.00 kV
WD = 10.5 mm
Signal A = SEI
Mag = 25.00 K X
1 µm
EHT = 10.00 kV
WD = 10.5 mm
Signal A = SEI
Mag = 20.00 K X
ZEISS

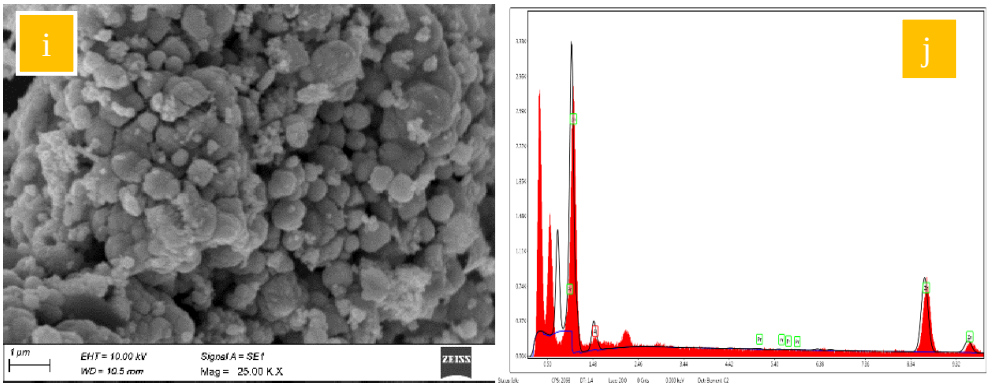



*Fig. 2. SEM & EDS images of:*
*a)b) Pristine ZnO; c) d) $Pr_{0.01}Al_{0.01}Zn_{0.98}O$; e) f) $Pr_{0.02}Al_{0.02}Zn_{0.96}O$;*
*g) h) $Pr_{0.03}Al_{0.03}Zn_{0.94}O$; i) j) $Pr_{0.04}Al_{0.04}Zn_{0.92}O$.*

### 3.3. Fourier Transform Infrared Spectroscopy (FTIR)

The method of FTIR spectroscopy was used in order to determine the functional groups that were present in the particles of generated mixed metal oxides. These particles included pure ZnO as well as ZnO NPs that had been doped with various quantities of Pr and Al. A fingerprint region of metal oxide nanoparticles was found, and its bandwidth was 716.17 $cm^{-1}$. The sharp peak at 1531 $cm^{-1}$ demonstrates that the C=O molecule is vibrating symmetrically. Both of these peaks were caused by water adsorption on the surface of zinc oxide nanoparticles, which resulted in the Zn-O stretching vibration at 3723 $cm^{-1}$ and the OH stretching bond vibration at 716.17 $cm^{-1}$. The wide peak at 3723 $cm^{-1}$ was attributed to the Zn-O stretching vibration, while the peak at 716.17 $cm^{-1}$ was caused by the OH stretching bond vibration. This is because of the vibration of the Pr,Al,Zn-O bonds, which was identified as a peak at a frequency of 716.17 $cm^{-1}$ over a range of Pr/Al codoped ZnO concentrations[18]. The reason for this is due to the fact that ZnO may be doped with varying amounts of Pr and Al. Differences in the peak shifts are what provide conclusive evidence of the existence of Pr and Al ions in the ZnO lattice at varied concentrations. These discrepancies can be observed up top. Mixed metal oxides are produced when two dopants, Pr and Al, are introduced into ZnO. This process causes the dopants to switch places with Zn atoms in the crystal lattice, which results in the development of mixed metal oxides.

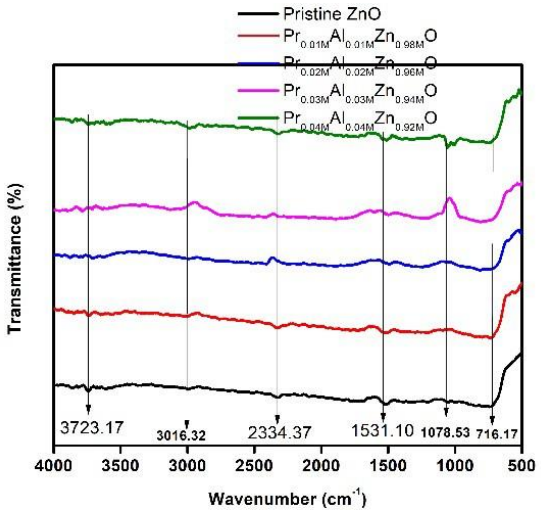



*Fig. 3. FTIR spectra of Pristine ZnO and Various concentrations of Pr and Al codoped ZnO.*

### 3.4. Ultraviolet-visible spectroscopy and bandgap calculation

The UV spectra of pure ZnO and Pr, Al-doped ZnO nanoparticles of various concentrations were determined with the use of ultraviolet spectroscopy (Figure 4). When the spectra of Pr, Al codoped ZnO nanoparticles are compared to those of pure ZnO, it is evident that the presence of these ions produces a blue shift in the absorption edge at shorter wavelengths. This can be seen clearly when comparing the two sets of spectra. The maximum absorbance of pure ZnO, as well as varying concentrations of Pr, Al-codoped ZnO NPs, can be found at 344, 344, 339, 342, and 344, respectively. When $Al^{3+}$ and $Pr^{2+}$ ions are introduced into ZnO NPs, the intensity of the peaks that are caused by the different ratios of Pr, Al-ZnO NPs is changed. Using the formula (hv)n =A(hv-Eg), the bandgap (fig 5) of pure ZnO and Pr, Al-doped ZnO NPs at varying concentrations was determined to be 3.10, 2.95, 2.81, 2.73, and 2.60 eV, respectively. The lower band gap values in Pr, Al codoped ZnO NPs were due to the higher concentration of $Pr^{2+}$ ions in the ZnO system[19]. The aforementioned viewpoints demonstrate that $Pr^{2+}$ ions and $Al^{3+}$ are successfully incorporated into the ZnO lattice.

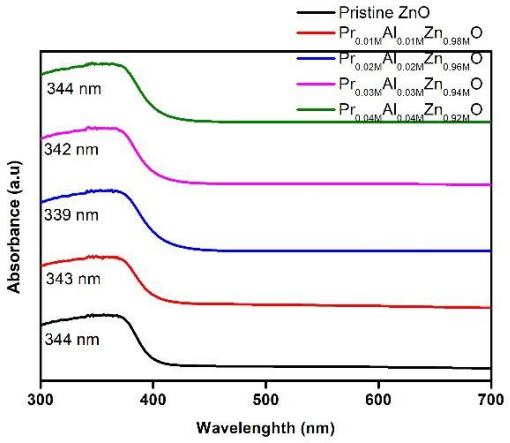



*Fig. 4. UV-Visible Spectra and bandgap for Pristine ZnO and different concentrations of Pr and Al codoped ZnO.*

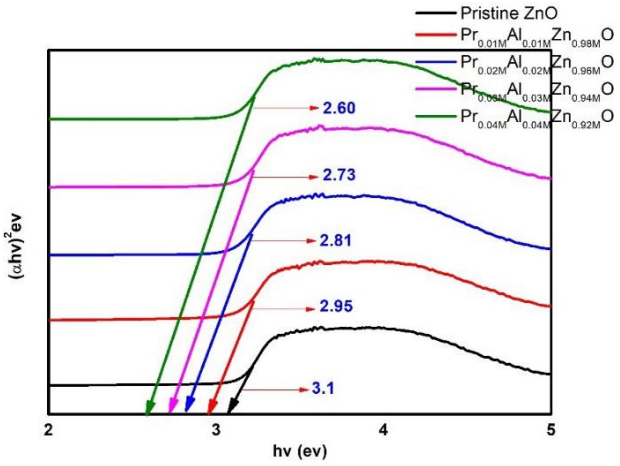



*Fig. 5. Bandgap for Pristine ZnO and different concentrations of Pr and Al codoped ZnO NPs.*

### 3.5. Photoluminescence spectra of Pr, Al-ZnO NPs

In Figure 6, the luminescence spectrum of pure ZnO as well as various concentrations of Pr, Al-doped ZnO NPs are shown. The spectrum displays four peaks that are comparable to the luminescence spectrum of pristine ZnO NPs. The first two peaks, located at 485 nm and 498 nm, are

the result of recombination between $e^{-}_{(CB)}$and $h^{+}_{(VB)}$, while the peaks located at 470 nm and 452 nm are the result of recombination between e- (CB) and h+ (VB). The intensity shift demonstrates that $Pr^{2+}$ and $Al^{3+}$ have been introduced into the ZnO system, and the wide peaks demonstrate that the synthesised Pr, Al-doped ZnO NPs contain less defects.

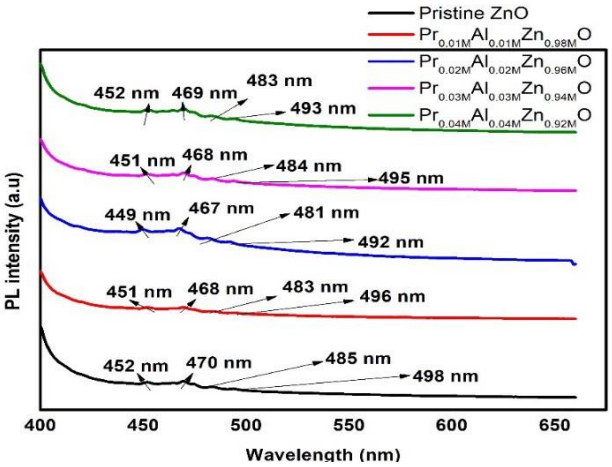



*Fig. 6. Photoluminescence image of Pristine ZnO and different concentrations of Pr and Al codoped ZnO NPs.*

## 4. Conclusion

Investigations using SEM-EDAX, FTIR, XRD, PL, and UV-Vis were carried out on the synthesized nanoparticles. The FTIR spectra of the ZnO nanocomposites in order to confirm that the Pr and Al included in the nanocomposites perform the functions for which they were designed. The absorption peak related to the ZnO stretching vibration (714 $cm^{-1}$). In the XRD patterns, a significant peak located at 34.5° indicated the presence of Pr and Al. This finding is consistent with the hypothesis that the ZnO NPs were in a polycrystalline phase and had a Wurtzite structure. In addition, the discovery of several ZnO crystal planes offered conclusive evidence that the NPs due to the interaction with the Pr and Al matrix. The bandgap values of pure zinc oxide, Pr and Al codoped zinc oxide with various amounts were found to be 3.10, 2.95, 2.81, 2.73, and 2.60 eV, respectively. It was discovered that the sizes of the particles were as 40.07, 38.65, 36.84, 38.87, and 39.91 nm. The nanosized ZnO particles were confirmed to have aggregated and distributed themselves across the whole Pr and Al nanosystem by scanning electron microscopy. In addition, the EDAX analysis demonstrated the sample's lack of impurities. According to the results of a UV-vis spectral investigation, the absorbance of pure ZnO and various concentrations of Pr and Al contained zinc oxide nanocomposites was increased and decreased, respectively. As shown by the concomitant intensity shift, PL spectroscopy provides conclusive evidence for the existence of $Pr^{2+}$ and $Al^{3+}$ in the ZnO system.

### Acknowledgments

This work was supported by the King Khalid University through a grant RCAMS/KKU/04-22 under the Research Center for Advance Materials (RCAMS) at King Khalid University, Saudi Arabia

## References

[1] Sharma, Dhirendra Kumar, Sweta Shukla, Kapil Kumar Sharma, and Vipin Kumar, Materials Today: Proceedings **49**, 3028-3035 (2022); https://doi.org/10.1016/j.matpr.2020.10.238
[2] Joesna.G, Saravanan.P, Zema.R, Ferin, Gunachitra.T, Sankar.D,Tamilselvan, Meena.M, Senthilkannan, Vimalan.M, and Gulam Mohamed, Journal of Materials Science: Materials in Electronics **33** (17) 14144-14158 (2022); https://doi.org/10.1007/s10854-022-08344-0
[3] Linghu, Jiajun, Tingting Song, Tong Yang, Jun Zhou, Kimyong Lim, Chornghaur Sow, Ming Yang, Yuanping Feng, and Xuezhi Wang, Materials Science in Semiconductor Processing **155,** 107237 (2023); https://doi.org/10.1016/j.mssp.2022.107237
[4] He, Haiping, Solution Processed Metal Oxide Thin Films for Electronic Applications, 7-30, (2020); https://doi.org/10.1016/B978-0-12-814930-0.00002-5
[5] Jeevanantham V, Tamilselvi D, Bavaji SR and Mohan S, Bulletin of Materials Science, 46 (1), 32 (2023); https://doi.org/10.1007/s12034-022-02868-1
[6] Shukla, Vipul J and Amit Patel, Molecular Crystals and Liquid Crystals, **712 (**1), 62-75, (2020); https://doi.org/10.1080/15421406.2020.1856505
[7] Guziewicz, Elzbieta, Tomasz Aleksander Krajewski, Ewa Przezdziecka, Krzysztof. P, Korona, Nikodem Czechowski, Lukasz Klopotowski, and Penka Terziyska. Physica Status Solidi B **257** (2), 1900472 (2020); https://doi.org/10.1002/pssb.201900472
[8] Narayana, Ashwath, Sachin Bhat, Almas Fathima, Lokesh.S.V, Sandeep.G. Surya, and Yelamaggad. C.V, RSC advances **10(23)**, 13532-13542 (2020); https://doi.org/10.1039/D0RA00478B
[9] Vinitha, Viswanathan, Mani Preeyanghaa, Vasudevan Vinesh, Ravikumar Dhanalakshmi, Bernaurdshaw Neppolian, and Vajiravelu Sivamurugan, Emergent Materials **4**,1093-1124 (2021); https://doi.org/10.1007/s42247-021-00262-x
[10] Jeevanantham V, Tamilselvi D, Rathidevi K and Bavaji SR, P Neelakandan, Biomass Conversion and Biorefinery, 1-10, https://doi.org/10.1007/s13399-023-04179-9
[11] Malhotra, Nemi, Hua-Shu Hsu, Sung-Tzu Liang, Marri Jmelou M. Roldan, Jiann-Shing Lee, Tzong-Rong Ger, and Chung-Der Hsiao, Animals **10(**9), 1663 (2020); https://doi.org/10.3390/ani10091663
[12] Manojkumar MS, Jeyajothi K, Jagadeesan A and Jeevanantham V, Journal of the Indian Chemical Society 99 (8), 100559 https://doi.org/10.1016/j.jics.2022.100559
[13] Dushyantha, Nimila, Nadeera Batapola, I. M. S. K. Ilankoon, Sudath Rohitha, Ranjith Premasiri, Bandara Abeysinghe, Nalin Ratnayake, and Kithsiri Dissanayake, Ore Geology Reviews, **122**, 103521 (2020); https://doi.org/10.1016/j.oregeorev.2020.103521
[14] Samrot, Antony.V, Chamarthy Sai Sahithya, Jenifer Selvarani, Sajna Keeyari Purayil, and Paulraj Ponnaiah, Current Research in Green and Sustainable Chemistry **4,**100042 (2021); https://doi.org/10.1016/j.crgsc.2020.100042
[15] Jeevanantham V, Tamilselvi D, Rathidevi K and Bavaji SR, Journal of Materials Research 38 (7), 1909-1918 https://doi.org/10.1557/s43578-023-00965-3
[16] Sreekanth.M, Ghosh.S, Mehta.SK, Ganguli AK, and Menaka Jha, CrystEngComm **19(**16), 2264-2270 (2017); https://doi.org/10.1039/C7CE00073A
[17] Madkour, Loutfy.H. Nanoelectronic materials: fundamentals and applications **116** (2019); https://doi.org/10.1007/978-3-030-21621-4_1
[18] Sathya V, Jagatheesan R, Jeevanantham V, Gopi D and Baby Shakila P, Journal of Applied Electrochemistry, 1-8 https://doi.org/10.1007/s10800-023-01890-3
[19] Madkour, Loutfy H., and Loutfy H. Madkour. Nanoelectronic Materials: Fundamentals and Applications 701-759 (2019); https://doi.org/10.1007/978-3-030-21621-4_17